Check for updates

Geophysical Research Letters

RESEARCH LETTER
10.1029/2025GL118740

Physics or Knob-Tuning? Tropical Anvil Peak Is Captured by GCMs

Youtong Zheng[1,2], Nadir Jeevanjee[3], Pu Lin[3], David Paynter[3], and Zhihong Tan[4]

[1]Department of Earth and Atmospheric Science, University of Houston, Houston, TX, USA, [2]Institute of Climate and Atmospheric Science, University of Houston, Houston, TX, USA, [3]NOAA/Geophysical Fluid Dynamics Lab, Princeton, NJ, USA, [4]Atmospheric and Oceanic Science Program, Princeton University, Princeton, NJ, USA

Key Points:

- General Circulation Models robustly capture the observed tropical anvil cloud peak near 200 hPa, despite debates on model realism and parameterization tuning
- Using Geophysical Fluid Dynamics Laboratory (GFDL) AM4 with cloud fraction schemes ranging from prognostic to binary, we consistently reproduce the tropical anvil cloud peak
- The anvil cloud peak emerges naturally due to frequent saturation events driven by minimal saturation deficits at cold upper levels

Supporting Information:

Supporting Information may be found in the online version of this article.

Correspondence to:

Y. Zheng,
yzheng18@uh.edu

Citation:

Zheng, Y., Jeevanjee, N., Lin, P., Paynter, D., & Tan, Z. (2025). Physics or knob-tuning? Tropical anvil peak is captured by GCMs. *Geophysical Research Letters*, *52*, e2025GL118740. https://doi.org/10.1029/2025GL118740

Received 25 AUG 2025
Accepted 13 OCT 2025

© 2025 The Author(s).
This is an open access article under the terms of the Creative Commons Attribution-NonCommercial License, which permits use, distribution and reproduction in any medium, provided the original work is properly cited and is not used for commercial purposes.

Abstract Tropical anvil clouds peak near 200 hPa and significantly impact Earth's climate, yet its physical realism in coarse-resolution General Circulation Models (GCMs) remains debated. We examine anvil cloud formation by performing simulations with a GCM with a hierarchy of cloud fraction schemes ranging from a complex prognostic Tiedtke scheme to a simple binary scheme. All schemes consistently reproduce the anvil peak. The robust anvil peak arises because extremely cold temperatures at the upper troposphere facilitate frequent saturation events, producing clouds that disproportionately influence mean cloud fraction. Sensitivity experiments with enhanced evaporation of cloud condensate unexpectedly show increased anvil coverage, highlighting how slight evaporative moistening reinforces local saturation in cold upper-tropospheric conditions. These results demonstrate that the tropical anvil cloud peak emerges from fundamental thermodynamic constraints, rather than specific cloud fraction parameterization choices.

Plain Language Summary Tropical anvil clouds form at high altitudes around 12 km (about 7.5 miles) above Earth's surface and strongly influence climate by affecting heat and radiation. Scientists question whether climate models accurately represent these clouds. To investigate this, we used a climate model with various methods for calculating cloud cover, from complex to very simple. Surprisingly, all methods showed a similar peak in anvil cloud occurrence at this altitude. This occurs because extremely cold temperatures at these heights often cause air to saturate, creating frequent cloud formation. Additionally, experiments revealed that increasing evaporation of cloud droplets unexpectedly increased cloud coverage by adding moisture that maintains saturation. Our study highlights that the tropical anvil cloud peak results mainly from basic atmospheric conditions, rather than specific modeling choices.

1. Introduction

Tropical anvil clouds, typically peaking around 200 hPa, exert a profound influence on Earth's climate system (Hartmann et al., 2001; Houze & Betts, 1981; Stephens et al., 2008). Their widespread coverage and persistence make anvil clouds a key component of cloud feedback mechanisms and climate sensitivity (Hartmann et al., 2001; Stephens et al., 2008; Zelinka et al., 2013, 2022), yet there remains substantial uncertainty regarding their governing processes and response to global warming (Zelinka et al., 2022).

Observational and modeling studies suggest that anvil cloud coverage decreases with warming (Beydoun et al., 2021; Bony et al., 2016; Raghuraman et al., 2024; Saint-Lu et al., 2020; Tompkins & Craig, 1999; Williams & Pierrehumbert, 2017), a finding consistent with the negative anvil area feedback assessed by the World Climate Research Program (Sherwood et al., 2020). The prevailing explanation for this behavior is the stability-iris mechanism (Bony et al., 2016). This mechanism proposes that as the climate warms, enhanced upper-tropospheric stability suppresses convective outflow, leading to a reduction in anvil cloud fraction. The conceptual foundation for this mechanism was established by Hartmann and Larson (2002) who find that convective cloudy air masses pile up near the 200 hPa level, where clear-sky radiative cooling diminishes so that the convective air masses must cease to rise to ensure steady-state energy balance (Kuang & Hartmann, 2007; Kubar et al., 2007). This mechanism, however, was challenged by Seeley et al. (2019) who used a cloud-resolving model and a simple theory to argue that the major cause of the anvil cloud peak is their long lifetime caused by slow evaporation of cloud condensates, instead of the detrainment from the convective outflow. As such, the reasons behind the formation of anvil coverage remain uncertain, as echoed by Zelinka et al. (2022)'s remarks "*Much*

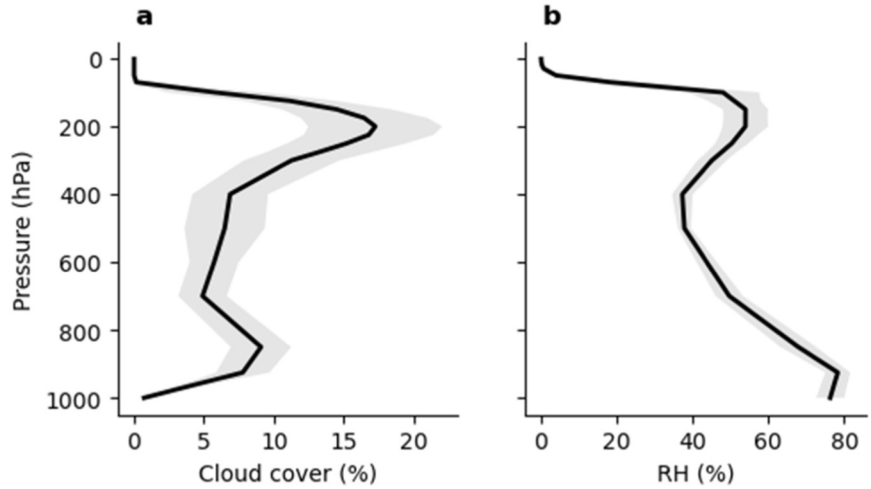


Figure 1. Profiles of (a) tropical cloud fraction and (b) relative humidity, averaged between 30°S and 30°N, from the Atmospheric Model Intercomparison Project output in the Climate Model Intercomparison Project Phase 6 archive. The gray shadings represent the standard deviations.

uncertainty remains surrounding the processes controlling tropical anvil cloud fraction and its changes with warming, and the fidelity with which General Circulation Models (GCMs) can simulate them."

Despite these uncertainties, GCMs robustly reproduce a peak in anvil cloud fraction around 200 hPa (Figure 1a). Given the parameterized nature of cloud processes in GCMs, this agreement is not trivial. Most cloud fraction parameterization schemes diagnose cloud fraction by assuming a probability density function (PDF) to represent subgrid-scale variability of total water content (Tompkins, 2005), linking cloud formation to relative humidity (RH). Yet, Climate Model Intercomparison Project Phase 6 (CMIP6) models exhibit bottom-heavy RH profiles that peak in the lower troposphere rather than at upper levels (Figure 1b). This indicates that the abundance of clouds near anvil altitudes is disproportionally large relative to what would be inferred from the RH profile at lower levels. This discrepancy prompts a question: Does the anvil cloud fraction peak result from artificial knob tuning, such as adjusting critical RH thresholds (Quaas, 2012), or does it arise naturally from basic physical constraints inherent to GCMs?

To address this question, we investigate the constraints governing anvil cloud fraction by conducting experiments using the latest version of the Geophysical Fluid Dynamics Laboratory (GFDL) atmospheric model, AM4. AM4 is particularly suited for this analysis due to its prognostic cloud fraction scheme (Tiedtke, 1993), explicitly simulating the balance between cloud fraction sources and sinks, including mixing with ambient unsaturated air, in a manner consistent with Seeley et al. (2019)'s theory. By varying the cloud fraction scheme in a hierarchical manner, we assess whether anvil cloud fraction remains robustly simulated and identify the fundamental physical principles driving its formation.

2. Model and Simulations

2.1. GFDL Atmosphere Model

We use GFDL's latest atmosphere climate model, AM4 (Zhao et al., 2018). AM4 has a horizontal resolution of ∼100 km, with 33 vertical model levels. It adopts the dynamic core from the hydrostatic version of the GFDL Finite-Volume Cubed-Sphere Dynamical Code (FV3) (Harris et al., 2020; Lin, 2004). AM4 uses a "double-plume" convective closure scheme to parameterize both shallow and deep convection (Zhao et al., 2018). The boundary layer scheme is based on Lock et al. (2000). The cloud microphysics scheme is primarily based on the works of Rotstayn (1997) and Jakob and Klein (2000). The cloud macrophysics scheme is a fully prognostic scheme originally developed by Tiedtke (1993). The scheme has two cloud sources of large-scale condensation and parameterized convection, one cloud sink of erosion, and two distribution terms of horizontal advection and vertical mixing, which move the clouds as passive tracers but do not generate or dissipate cloudiness.

19448007, 2025, 20, Downloaded from https://agupubs.onlinelibrary.wiley.com/doi/10.1029/2025GL118740 by Youtong Zheng - University Of Houston Library , Wiley Online Library on [27/10/2025]. See the Terms and Conditions (https://onlinelibrary.wiley.com/terms-and-conditions) on Wiley Online Library for rules of use; OA articles are governed by the applicable Creative Commons License

19448007, 2025, 20, Downloaded from https://agupubs.onlinelibrary.wiley.com/doi/10.1029/2025GL118740 by Youtong Zheng - University Of Houston Library , Wiley Online Library on [27/10/2025]. See the Terms and Conditions (https://onlinelibrary.wiley.com/terms-and-conditions) on Wiley Online Library for rules of use; OA articles are governed by the applicable Creative Commons License

2.2. Experiments

All simulations were performed with prescribed sea surface temperature, sea ice, greenhouse gas, and aerosols, with their climatological monthly mean values centered in 2010. To ensure clean comparisons between different cloud fraction schemes, the simulations are nudged to the Modern-Era Retrospective analysis for Research and Applications, Version 2 (MERRA2) reanalysis meteorology (wind, temperature, and specific humidity), with a nudging timescale of 30 min. The experiment runs for 2 years, and the second year is used for analysis. We also tested the results with 30-year free-running simulations and found similar results (Figure S2 in Supporting Information S1).

We performed simulations using three distinct cloud fraction parameterization schemes:

1. Prognostic scheme (Tiedtke, 1993): The default AM4 cloud fraction scheme, which explicitly models cloud formation and dissipation including a cloud sink due to lateral mixing of cloud condensate with unsaturated air. The mixing rates scale proportionally to the saturation deficit-to-cloud water ratio, aligning with the theoretical framework of Seeley et al. (2019). A major source term is the large-scale condensation (lsc), which initiates when net cooling occurs, and the RH exceeds a height-dependent threshold (~80% on average). Testing with a fixed threshold shows a similar cloud fraction profile (not shown).
2. PDF-based diagnostic scheme (Tompkins, 2005): This scheme assumes a symmetric beta function to describe the subgrid-scale distribution of total water content, linking cloud fraction to RH. This scheme is broadly representative of standard cloud fraction schemes in most GCMs.
3. Binary scheme: A grid cell is either fully cloudy (100%) or entirely clear (0%), based solely on whether the total water content exceeds saturation. It can be considered as a "cloud resolving" version of the coarse-gridded AM4. The binary scheme is the simplest one, helping us to interpret the results.

2.3. Cloud Fraction Decomposition

To obtain process-level insights, we decompose the mean cloud fraction ($\overline{\mathrm{CF}}$):

$$\overline{\mathrm{CF}} = \overline{\mathrm{CF}_{\mathrm{lsc}}} + \overline{\mathrm{CF}_{\mathrm{nolsc}}} \tag{1a}$$

$$\overline{\mathrm{CF}_{\mathrm{lsc}}} = \frac{1}{n}\sum_{t=1}^{n} \mathcal{H}[C(t)] \cdot \mathrm{CF}(t) \tag{1b}$$

$$\overline{\mathrm{CF}_{\mathrm{nolsc}}} = \frac{1}{n}\sum_{t=1}^{n} (1 - \mathcal{H}[C(t)]) \cdot \mathrm{CF}(t) \tag{1c}$$

in which the "lsc" denotes conditions with large-scale condensation of water vapor, while "nolsc" indicates those without, and the overbar represents time average over n model time steps. The $\mathcal{H}$ is the Heaviside function and $C(t)$ is the condensation indicator: $C(t) > 0$ if condensation occurs. In the Tiedtke scheme, condensation rate is a budget term so the $C(t)$ is readily determined. In binary and PDF schemes, the $C(t) > 0$ if the air reaches saturation and cloud water increases after execution of cloud fraction calculation.

Note that clouds generated from condensation by convective parameterization are grouped under the "nolsc" category, which is small at most levels except in the boundary layer (Figure S2 in Supporting Information S1).

Physically, $\mathrm{CF}_{\mathrm{lsc}}$ represents actively forming clouds in saturated or near-saturated air experiencing upward motion (Figure S3 in Supporting Information S1). In the free troposphere, where the contribution from parameterized convection is minor, $\mathrm{CF}_{\mathrm{nolsc}}$ represents passive clouds sustained or dissipating mostly within unsaturated ambient air (Figure S3 in Supporting Information S1). To the first order, the $\mathrm{CF}_{\mathrm{nolsc}}$ can be considered residues of previously formed $\mathrm{CF}_{\mathrm{lsc}}$.

3. Results

Figure 2 shows the vertical profiles of tropical cloud fraction from the three simulations with different cloud fraction schemes. Regardless of the scheme employed, the simulations consistently produce a top-heavy cloud fraction profile, with the anvil cloud peak at ~200 hPa appearing even with the simplest binary cloud fraction

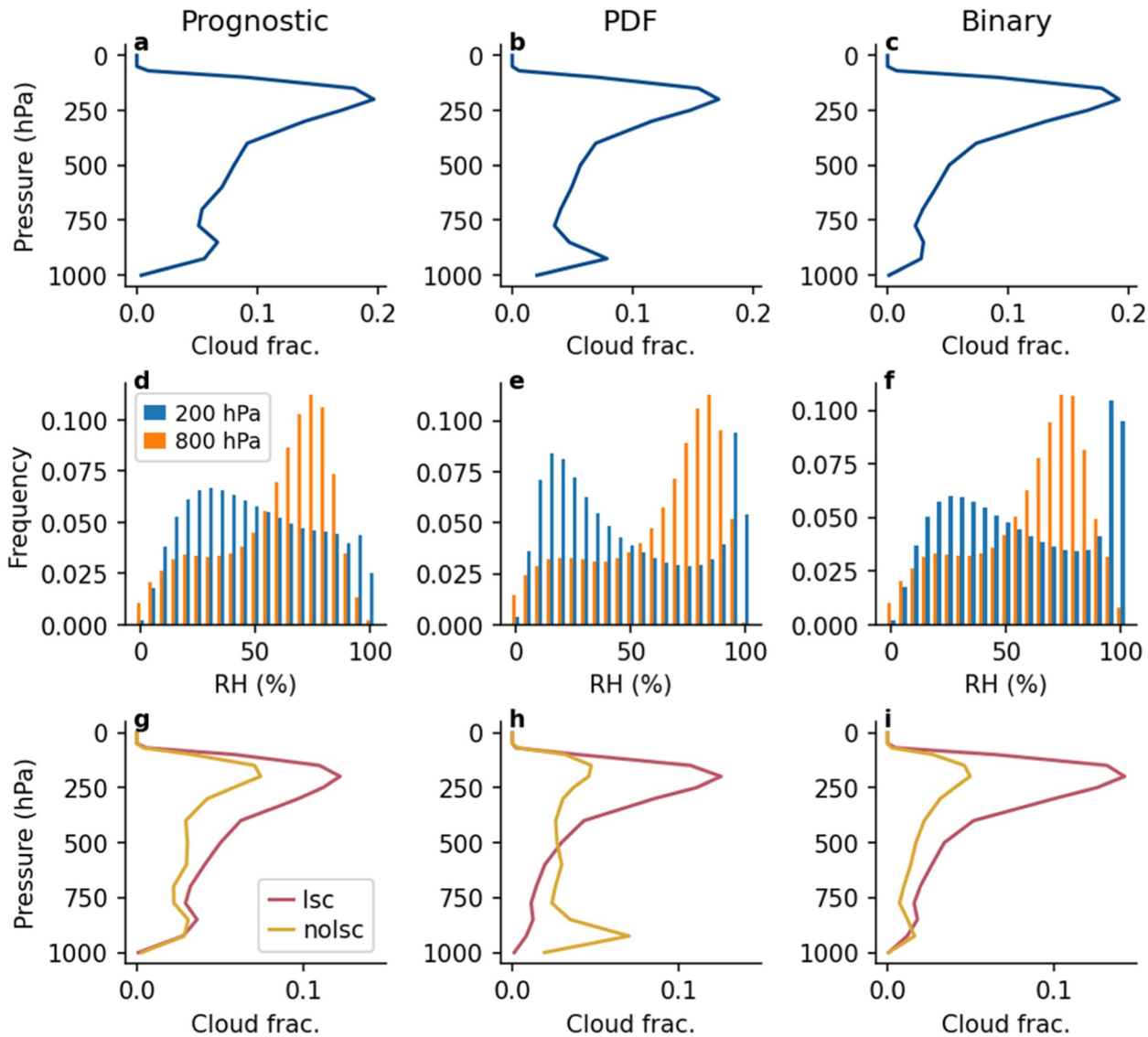


Figure 2. Simulated profiles of tropical cloud fraction (upper), histogram of relative humidity (RH) at 200 and 800 hPa levels (middle), and decomposition of total cloud fraction into $\overline{CF_{lsc}}$ and $\overline{CF_{nolsc}}$ (bottom) with prognostic (left), PDF-based diagnostic (middle), and binary (right) cloud fraction parameterizations. The variables are averaged from 30°S to 30°N. The histograms of RH are based on instantaneous 3-hourly output.

scheme. This suggests that tuning of cloud fraction schemes is not required to reproduce the anvil peak; rather, fundamental physical constraints are responsible for its formation.

To understand how the anvil peak is simulated, we first focus on the binary cloud scheme simulation (right panel of Figure 2) because of its interpretability and ability to reproduce the anvil peak. We analyze 3-hourly instantaneous cloud fraction and RH at two levels: 200 hPa (the anvil level) and 800 hPa (a lower tropospheric level with significantly smaller cloud fraction). Unlike the 800 hPa level, where RH exhibit a relatively narrow distribution with a dominant peak near 80%, the 200 hPa level shows a broader distribution with a notably higher frequency of saturation events (Figure 2f). $\overline{CF_{lsc}}$ dominates the cloud cover at higher levels, resulting in the anvil peak (Figure 2i). Thus, the anvil cloud fraction primarily depends on the frequency of high-RH episodes rather than mean RH values.

This behavior persists in the PDF cloud scheme (middle column of Figure 2). The top-heavy cloud fraction is predominantly driven by the $\overline{CF_{lsc}}$ (Figure 2h). At lower levels, the PDF scheme allows clouds to form under unsaturated environments, leading to larger $\overline{CF_{nolsc}}$ than the binary scheme.

19448007, 2025, 20, Downloaded from https://agupubs.onlinelibrary.wiley.com/doi/10.1029/2025GL118740 by Youtong Zheng - University Of Houston Library , Wiley Online Library on [27/10/2025]. See the Terms and Conditions (https://onlinelibrary.wiley.com/terms-and-conditions) on Wiley Online Library for rules of use; OA articles are governed by the applicable Creative Commons License

19448007, 2025, 20, Downloaded from https://agupubs.onlinelibrary.wiley.com/doi/10.1029/2025GL118740 by Youtong Zheng - University Of Houston Library , Wiley Online Library on [27/10/2025]. See the Terms and Conditions (https://onlinelibrary.wiley.com/terms-and-conditions) on Wiley Online Library for rules of use; OA articles are governed by the applicable Creative Commons License

For the prognostic cloud scheme, $\overline{CF_{lsc}}$ remains the primary contributor to the top-heavy distribution, although the role of $\overline{CF_{nolsc}}$ is larger compared to those in diagnostic schemes. Unlike diagnostic schemes in which cloud fraction responds to the ambient environment relatively quickly, prognostic clouds possess more "memory" of prior atmospheric conditions. The frequency of saturation events at 200 hPa in the prognostic scheme is lower compared to other schemes, partially because condensation occurs at an RH threshold of ∼80%, thus limiting moisture accumulation. Raising this threshold to 100% increases the saturation frequency (Figure S4 in Supporting Information S1). Nevertheless, even with lower saturation frequency, the prognostic scheme still produces a greater number of high-RH events at 200 hPa to support significant CF_{lsc} generation.

In summary, the GCM-simulated anvil cloud fraction is chiefly governed by the frequency of high-RH events rather than mean RH values, because of the nonlinear dependence of cloud fraction on RH.

Frequent upper-level saturation results primarily from non-local convective moistening, transporting moisture from lower atmospheric levels into colder upper tropospheric regions, where small saturation deficits allow easy saturation (e.g., Seeley et al., 2019). To gain physical intuition, we examine snapshots of RH, cloudiness, and omega at 200 and 800 hPa (Figure S5 in Supporting Information S1). At 200 hPa, ascending motions consistently result in saturation and high cloudiness, whereas at 800 hPa, the correspondence between ascent and high-RH regions is notably weaker. To further quantify this process, we perform conditional sampling of ascent events (defined by omega <-0.05 Pa/s) and track the evolutions from 7 days before to 7 days after the omega perturbation (Figure S6 in Supporting Information S1). It shows that RH increases at 200 hPa are nearly twice those at 800 hPa following a similar ascent perturbation (Figure S6 in Supporting Information S1). This difference in moistening magnitude aligns with a simple analytical calculation based on simulated temperature and its lapse rate (Text S1 in Supporting Information S1), underscoring the enhanced susceptibility of upper-level cold air to moistening.

4. Extending Seeley et al. (2019)'s Theory to GCM

Seeley et al. (2019) proposed, using a convection-permitting model, that anvil peak is formed by slow evaporation of cloud condensate at the anvil level where the low saturation deficit significantly limits evaporation, thereby prolonging cloud lifetime. Our analysis not only supports this mechanism but also extends its validity to a traditional coarse-resolution GCM with parameterized cloud processes. Specifically, the high frequency of high-RH events at the anvil level naturally disfavors cloud evaporation, reinforcing anvil cloud persistence.

To confirm this idea, we analyze the evaporation rate, E (g/kg/day), normalized by cloud water content, q_c (g/kg), as a measure of evaporation efficiency in depleting cloud water (Figures 3a–3c). The E/q_c decreases rapidly with altitude, consistent with Seeley et al. (2019)'s slow-evaporation argument. At the anvil level, the evaporation rate is sufficiently low to sustain high cloud fraction, with precipitation acting as the primary sink of anvil cloud condensate (red lines in Figures 3d–3f). At lower levels, evaporation becomes a dominant cloud sink, comparable to or exceeding precipitation as the major sink term—again in agreement with Seeley et al. (2019) (their Figure 4b). Notably, the slow evaporation of anvil clouds is independent of the cloud fraction parameterization. The prognostic cloud scheme explicitly parameterizes the evaporation as a function of saturation deficit while the diagnostic and binary schemes do not. Despite these differences, all schemes robustly simulate the slow evaporation mechanism, indicating that the microphysical details of evaporation are not the most determinant factor.

To further probe this mechanism, we conduct sensitivity experiments by applying a scaling factor of 2 to the evaporation term in the Tiedtke scheme. As expected, this scaling enhanced E/q_c across all levels (Figure 4a), generally reducing cloud fraction at most levels. However, notably at the anvil peak (∼200 hPa), cloud fraction slightly increased despite enhanced evaporation (Figure 4b). This somewhat counterintuitive result can be explained by subtle interplay between evaporation and local saturation. At 200 hPa, even minor additional moistening from enhanced evaporation rates can readily saturate the extremely cold air (Figure 4c), consequently increasing the frequency of condensation and thus cloud coverage.

Seeley et al. (2019) questioned GCMs' capability to capture this mechanism, noting that "*Most GCMs do not account for vertically varying cloud sinks in their computation of cloud fraction*; for example*, the most common type of cloud-fraction parameterization used in the combined CMIP3/CMIP5 ensemble is based on a diagnostic function of RH alone*." Our results address this concern, demonstrating that the slow evaporation mechanism

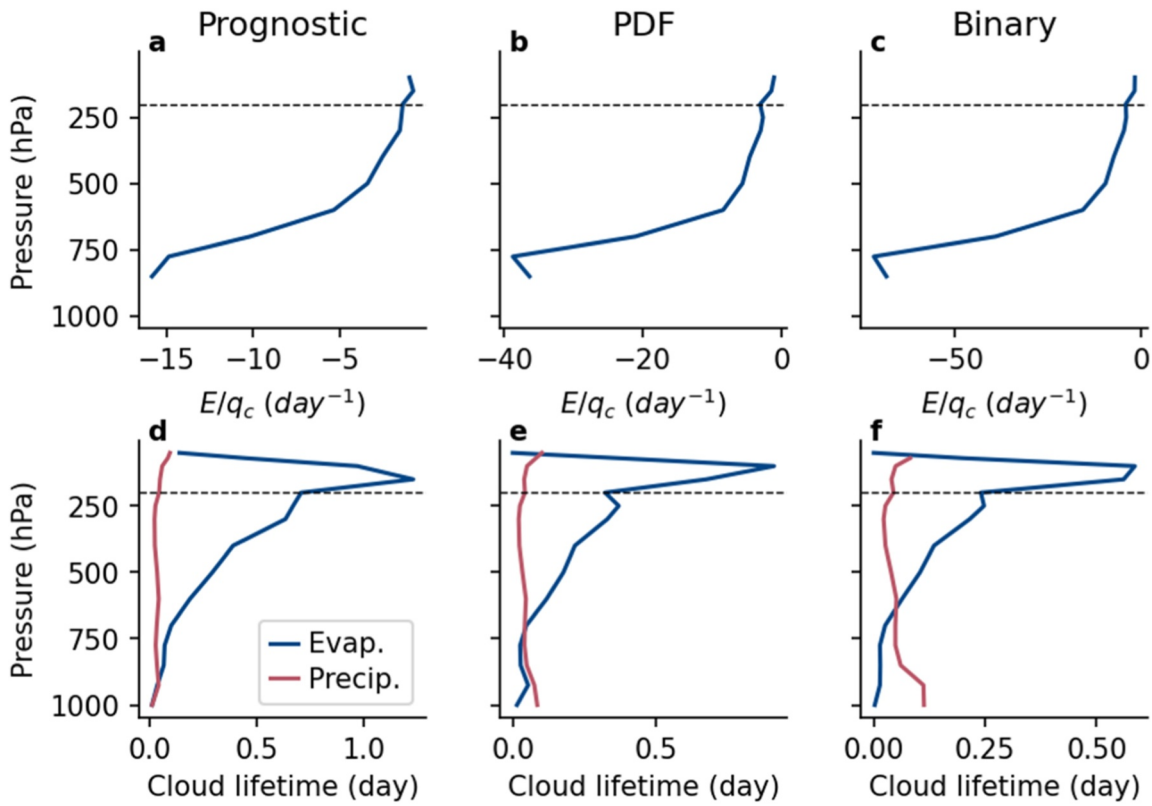


Figure 3. AM4 simulated profiles of E/q_c (upper), and estimated cloud lifetimes (bottom) with prognostic (left), PDF-based diagnostic (middle), and binary (right) cloud schemes, averaged between 30°S and 30°N. The same visualization with the same *x*-axis limits for all panels is shown in Figure S7 in Supporting Information S1. The cloud lifetime due to the evaporation and precipitation are computed via dividing the q_c by the E and the precipitation rate (g/kg/day), respectively. In the prognostic scheme, E is directly available as a budget term, while in diagnostic schemes, it is computed from any decrease in cloud water (if present) in each time step after the cloud fraction calculation.

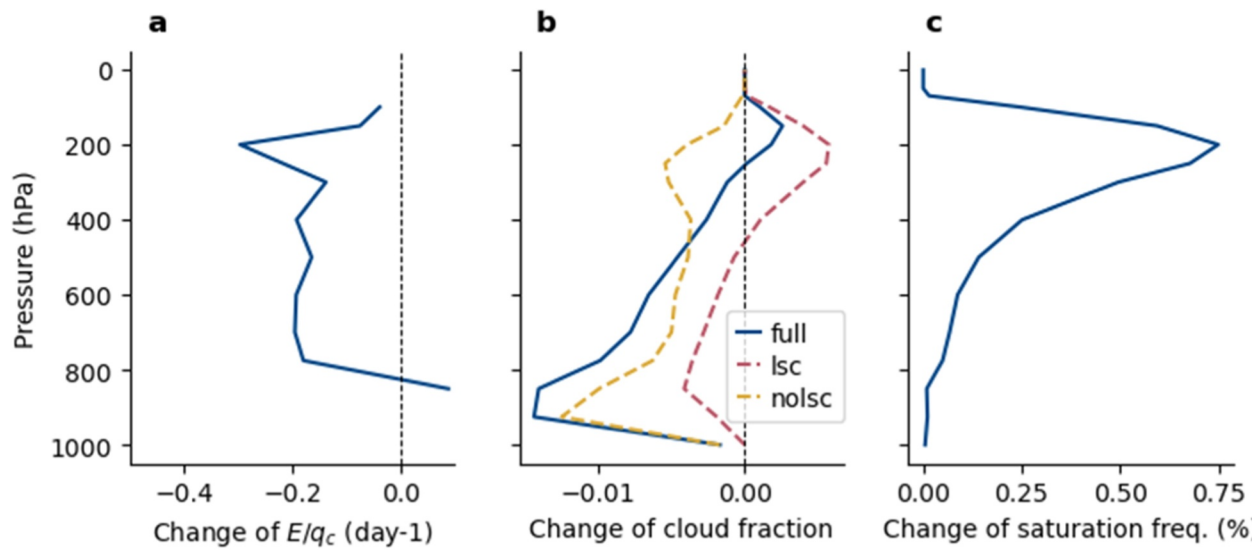


Figure 4. Profiles of simulated changes in (a) E/q_c, (b) cloud fraction, and (c) frequency of supersaturation in the sensitivity experiment. Note that the relative changes are quite small; it is their shape, not their magnitude, that conveys the key point.

19448007, 2025, 20, Downloaded from https://agupubs.onlinelibrary.wiley.com/doi/10.1029/2025GL118740 by Youtong Zheng - University Of Houston Library , Wiley Online Library on [27/10/2025]. See the Terms and Conditions (https://onlinelibrary.wiley.com/terms-and-conditions) on Wiley Online Library for rules of use; OA articles are governed by the applicable Creative Commons License

19448007, 2025, 20, Downloaded from https://agupubs.onlinelibrary.wiley.com/doi/10.1029/2025GL118740 by Youtong Zheng - University Of Houston Library , Wiley Online Library on [27/10/2025]. See the Terms and Conditions (https://onlinelibrary.wiley.com/terms-and-conditions) on Wiley Online Library for rules of use; OA articles are governed by the applicable Creative Commons License

emerges robustly from fundamental thermodynamic constraints inherently represented in coarse-gridded GCMs, independent of the specific cloud fraction parameterization details.

5. Concluding Remarks

Through a hierarchy of simulations using GFDL's AM4 with three distinct cloud fraction schemes, we find that the anvil cloud maximum, consistently observed in GCMs, arises fundamentally from the frequent occurrence of saturation events in the upper troposphere, rather than cloud fraction parameterization details. Our results are consistent with Seeley et al. (2019)'s theory that the minimal saturation deficit at these cold upper levels serves as a key constraint that limits the evaporation of cloud condensate by frequently generating saturation events. Sensitivity experiments further demonstrate that even when evaporation rates are artificially enhanced, anvil cloud fraction at ∼200 hPa remains resilient or even slightly increases, emphasizing a delicate interplay between evaporation and saturation conditions unique to the upper troposphere. These insights reinforce the notion that fundamental thermodynamic constraints, rather than the tuning of cloud fraction parameterization, primarily govern the tropical cloud fraction profile, contributing important clarity to the ongoing discourse regarding the physical realism of anvil cloud representation in GCMs (Seeley et al., 2019; Zelinka et al., 2022).

The thermodynamic mechanism highlighted in this study is not separate from the traditional view that convective detrainment shapes the anvil peak; rather the two are intrinsically coupled. The fundamental reason why cloud detrainment peaks at ∼200 hPa is the insufficient radiative emission of water vapor above this level, where saturation vapor pressure is extremely low due to the low temperatures. The low temperatures, in turn, help sustain anvil cloud condensate by creating an easy-to-saturate environment (our central takeaway). This coupling is consistent with Beydoun et al. (2021), who found that anvil cloud lifetime is linked to the clear-sky mass convergence. We therefore argue that future studies should treat the processes controlling the tropical anvil cloudiness as a fully coupled system, where both the formation of anvils through detrainment and their maintenance through low saturation deficit jointly determine anvil cloudiness and altitude. Such an approach will advance understanding of both anvil cloud area and altitude feedbacks.

Our study highlights three avenues for further investigation. First, while we emphasize the fundamental thermodynamic constraints responsible for the top-heavy distribution of cloud fraction, the role of cloud microphysical processes remains less explored. Beyond cloud fraction, microphysical details have stronger impact on cloud optical thickness, which critically influences the anvil cloud radiative feedback. Second, this study does not explain why the anvil peak cloud fraction consistently falls between 15% and 20% in both the CMIP6 models (Figure 1) and the AM4 experiments with different cloud-fraction schemes (Figures 2a–2c). Given the importance of thermodynamic constraint highlighted in this work, it should be feasible to develop a theoretical explanation for this characteristic anvil cloud fraction using basic principles such as Clausius-Clapeyron scaling and steady-state energy balance, similar to the approach of Romps (2014). Third, based on our experience with the AM4, we note that this model tends to generate a relatively high proportion of resolved convection than parameterized convection in the tropics, a characteristic that somewhat differentiates AM4 from many other GCMs. Future studies should therefore assess the robustness of our findings in other GCMs to generalize the findings.

Conflict of Interest

The authors declare no conflicts of interest relevant to this study.

Data Availability Statement

The CMIP5 data are available through the Earth System Grid Federation https://aims2.llnl.gov/. The NOAA GFDL AM4.0 model codes are available at https://github.com/NOAA-GFDL/AM4. The code and the AM4 simulation data are publicly available at Zenodo (Zheng, 2025).

Acknowledgments
We acknowledge NOAA GFDL provides computing resources used in this research. This work was initiated while YZ was at NOAA GFDL and continued at the University of Houston, where YZ is supported by the University of Houston Presidential Frontier Faculty startup fund and DOE Early Career Grant (DE-SC0024185). We thank two anonymous reviewers for their constructive comments. ChatGPT assisted in manuscript editing.

References

Beydoun, H., Caldwell, P. M., Hannah, W. M., & Donahue, A. S. (2021). Dissecting anvil cloud response to sea surface warming. *Geophysical Research Letters*, *48*(15), e2021GL094049. https://doi.org/10.1029/2021GL094049

Bony, S., Stevens, B., Coppin, D., Becker, T., Reed, K. A., Voigt, A., & Medeiros, B. (2016). Thermodynamic control of anvil cloud amount. *Proceedings of the National Academy of Sciences of the United States of America*, *113*(32), 8927–8932. https://doi.org/10.1073/pnas.1601472113

Harris, L., Zhou, L., Lin, S. J., Chen, J. H., Chen, X., Gao, K., et al. (2020). GFDL SHiELD: A unified system for weather-to-seasonal prediction. *Journal of Advances in Modeling Earth Systems*, *12*(10), e2020MS002223.

Hartmann, D. L., & Larson, K. (2002). An important constraint on tropical cloud - Climate feedback. *Geophysical Research Letters*, *29*(20), 12-1–12-14. https://doi.org/10.1029/2002GL015835

Hartmann, D. L., Moy, L. A., & Fu, Q. (2001). Tropical convection and the energy balance at the top of the atmosphere. *Journal of Climate*, *14*(24), 4495–4511. https://doi.org/10.1175/1520-0442(2001)014<4495:tcateb>2.0.co;2

Houze, R. A. Jr., & Betts, A. K. (1981). Convection in GATE. *Reviews of Geophysics*, *19*(4), 541–576. https://doi.org/10.1029/RG019i004p00541

Jakob, C., & Klein, S. A. (2000). A parametrization of the effects of cloud and precipitation overlap for use in general-circulation models. *Quarterly Journal of the Royal Meteorological Society*, *126*(568), 2525–2544. https://doi.org/10.1002/qj.49712656809

Kuang, Z., & Hartmann, D. L. (2007). Testing the fixed anvil temperature hypothesis in a cloud-resolving model. *Journal of Climate*, *20*(10), 2051–2057. https://doi.org/10.1175/JCLI4124.1

Kubar, T. L., Hartmann, D. L., & Wood, R. (2007). Radiative and convective driving of tropical high clouds. *Journal of Climate*, *20*(22), 5510–5526. https://doi.org/10.1175/2007JCLI1628.1

Lin, S.-J. (2004). A "Vertically Lagrangian" finite-volume dynamical core for global models. *Monthly Weather Review*, *132*(10), 2293–2307. https://doi.org/10.1175/1520-0493(2004)132<2293:AVLFDC>2.0.CO;2

Lock, A. P., Brown, A. R., Bush, M. R., Martin, G. M., & Smith, R. N. B. (2000). A new boundary layer mixing scheme. Part I: Scheme description and single-column model tests. *Monthly Weather Review*, *128*(9), 3187–3199. https://doi.org/10.1175/1520-0493(2000)128<3187:ANBLMS>2.0.CO;2

Quaas, J. (2012). Evaluating the "critical relative humidity" as a measure of subgrid-scale variability of humidity in general circulation model cloud cover parameterizations using satellite data. *Journal of Geophysical Research*, *117*(D9), D09208. https://doi.org/10.1029/2012JD017495

Raghuraman, S. P., Medeiros, B., & Gettelman, A. (2024). Observational quantification of tropical high cloud changes and feedbacks. *Journal of Geophysical Research: Atmospheres*, *129*(7), e2023JD039364. https://doi.org/10.1029/2023JD039364

Romps, D. M. (2014). An analytical model for tropical relative humidity. *Journal of Climate*, *27*(19), 7432–7449. https://doi.org/10.1175/jcli-d-14-00255.1

Rotstayn, L. D. (1997). A physically based scheme for the treatment of stratiform clouds and precipitation in large-scale models. I: Description and evaluation of the microphysical processes. *Quarterly Journal of the Royal Meteorological Society*, *123*(541), 1227–1282. https://doi.org/10.1002/qj.49712354106

Saint-Lu, M., Bony, S., & Dufresne, J.-L. (2020). Observational evidence for a stability iris effect in the tropics. *Geophysical Research Letters*, *47*(14), e2020GL089059. https://doi.org/10.1029/2020GL089059

Seeley, J. T., Jeevanjee, N., Langhans, W., & Romps, D. M. (2019). Formation of tropical anvil clouds by slow evaporation. *Geophysical Research Letters*, *46*(1), 492–501.

Sherwood, S. C., Webb, M. J., Annan, J. D., Armour, K. C., Forster, P. M., Hargreaves, J. C., et al. (2020). An assessment of Earth's climate sensitivity using multiple lines of evidence. *Reviews of Geophysics*, *58*(4), e2019RG000678. https://doi.org/10.1029/2019RG000678

Stephens, G. L., Vane, D. G., Tanelli, S., Im, E., Durden, S., Rokey, M., et al. (2008). CloudSat mission: Performance and early science after the first year of operation. *Journal of Geophysical Research*, *113*(D8), D00A18. https://doi.org/10.1029/2008JD009982

Tiedtke, M. (1993). Representation of clouds in large-scale models. *Monthly Weather Review*, *121*(11), 3040–3061. https://doi.org/10.1175/1520-0493(1993)121<3040:ROCILS>2.0.CO;2

Tompkins, A. M. (2005). The parametrization of cloud cover. *ECMWF Moist Processes Lecture Note Series Tech. Memo*, *25*.

Tompkins, A. M., & Craig, G. C. (1999). Sensitivity of tropical convection to sea surface temperature in the absence of large-scale flow. *Journal of Climate*, *12*(2), 462–476. https://doi.org/10.1175/1520-0442(1999)012<0462:sotcts>2.0.co;2

Williams, I. N., & Pierrehumbert, R. T. (2017). Observational evidence against strongly stabilizing tropical cloud feedbacks. *Geophysical Research Letters*, *44*(3), 1503–1510. https://doi.org/10.1002/2016GL072202

Zelinka, M. D., Klein, S. A., Qin, Y., & Myers, T. A. (2022). Evaluating climate models' cloud feedbacks against expert judgment. *Journal of Geophysical Research: Atmospheres*, *127*(2), e2021JD035198. https://doi.org/10.1029/2021JD035198

Zelinka, M. D., Klein, S. A., Taylor, K. E., Andrews, T., Webb, M. J., Gregory, J. M., & Forster, P. M. (2013). Contributions of different cloud types to feedbacks and rapid adjustments in CMIP5. *Journal of Climate*, *26*(14), 5007–5027. https://doi.org/10.1175/JCLI-D-12-00555.1

Zhao, M., Golaz, J., Held, I. M., Guo, H., Balaji, V., Benson, R., et al. (2018). The GFDL global atmosphere and land model AM4.0/LM4.0: 2. Model description, sensitivity studies, and tuning strategies. *Journal of Advances in Modeling Earth Systems*, *10*(3), 735–769. https://doi.org/10.1002/2017MS001209

Zheng, Y. (2025). Supporting data for "Physics or Knob-Tuning? Tropical Anvil Peak is Captured by GCMs" (version v1) [Dataset]. *Zenodo*. https://doi.org/10.5281/zenodo.16943830

19448007, 2025, 20, Downloaded from https://agupubs.onlinelibrary.wiley.com/doi/10.1029/2025GL118740 by Youtong Zheng - University Of Houston Library , Wiley Online Library on [27/10/2025]. See the Terms and Conditions (https://onlinelibrary.wiley.com/terms-and-conditions) on Wiley Online Library for rules of use; OA articles are governed by the applicable Creative Commons License